Direct Measurement of Hydrogen Dislocation Pipe Diffusion in Deformed Polycrystalline Pd Using Quasielastic Neutron Scattering

Brent J. Heuser,[1*] Dallas R. Trinkle,[2] Niina Jalarvo,[3,4] Joseph Serio,[1]
Emily J. Schiavone,[2] Eugene Mamontov,[3] and Madhusudan Tyagi[5,6]
[1]*Department of Nuclear, Plasma, and Radiological Engineering, University of Illinois, Urbana, Illinois 61801, USA*
[2]*Department of Materials Science and Engineering, University of Illinois, Urbana, Illinois 61801, USA*
[3]*Chemical and Engineering Materials Division, Neutron Sciences Directorate, Oak Ridge National Laboratory, Oak Ridge, Tennessee 37831, USA*
[4]*Juelich Centre for Neutron Science, Outstation at the Spallation Neutron Source, Oak Ridge National Laboratory, Oak Ridge, Tennessee 37831, USA*
[5]*National Institute of Standards and Technology Center for Neutron Research, Gaithersburg, Maryland 20899, USA*
[6]*Department of Materials Science and Engineering, University of Maryland, College Park, Maryland 20742, USA*
(Received 22 March 2014; published 10 July 2014)

The temperature-dependent diffusivity $D(T)$ of hydrogen solute atoms trapped at dislocations—dislocation pipe diffusion of hydrogen—in deformed polycrystalline PdH_x ($x \sim 10^{-3}$ [H]/[Pd]) has been quantified with quasielastic neutron scattering between 150 and 400 K. We observe diffusion coefficients for trapped hydrogen elevated by one to two orders of magnitude above bulk diffusion. Arrhenius diffusion behavior has been observed for dislocation pipe diffusion and regular bulk diffusion, the latter in well-annealed polycrystalline Pd. For regular bulk diffusion of hydrogen in Pd we find $D(T) = D_0\exp(-E_a/kT) = 0.005\exp(-0.23\ \text{eV}/kT)\ \text{cm}^2/\text{s}$, in agreement with the known diffusivity of hydrogen in Pd. For hydrogen dislocation pipe diffusion we find $D(T) \simeq 10^{-5}\exp(-E_a/kT)\ \text{cm}^2/\text{s}$, where $E_a = 0.042$ and 0.083 eV for concentrations of 0.52×10^{-3} and 1.13×10^{-3} [H]/[Pd], respectively. *Ab initio* computations provide a physical basis for the pipe diffusion pathway and confirm the reduced barrier height.

DOI: 10.1103/PhysRevLett.113.025504 PACS numbers: 61.72.Dd, 61.05.fg, 66.30.Xj

Dislocation pipe diffusion (DPD) refers to enhanced atomic migration along dislocations attributed to a reduced activation barrier associated with lattice strain in the core and near-core environment. The process, which can increase the diffusivity by orders of magnitude, has broad applicability in crystalline solids. This is because dislocations are a common defect influencing a host of physical responses, and atomic migration drives many solid state phenomena, including phase transformations and dislocation climb. The concept of DPD originated with the work of Turnbull and Hoffman [1], Hart [2], Love [3], and Balluffi and co-workers [4–6]. This early work considered the effect of vacancy self-diffusion (VSD), enhanced at dislocations, on dislocation climb or other mass transport regulated processes.

The first quantification of dislocation pipe diffusion, at least in terms of a determination of activation energy and diffusion constant separate from regular lattice diffusion, was TEM characterization of void shrinkage in Al by Volin *et al.* [4]. This was interpreted as enhanced VSD along dislocations leading to accelerated shrinkage for voids connected by dislocations. Additionally, Kirchheim indirectly quantified a diffusivity interpreted as DPD near ambient temperature [7]. More recently, Legros *et al.* observed the influence of dislocation pipe diffusion on Si particle precipitation and dissolution in Al using *in situ* TEM [8]. A body of recent literature exists related to DPD, including advance computational work and studies considering transport-mediated dislocation climb [9–11]. The use of quasielastic neutron scattering (QENS) to study hydrogen diffusion in metals dates to the late 1960s and 1970s [12–15] and continues to more recent work [16]. The temperature dependence of the diffusivity associated with DPD, necessary to determine the activation energy, is difficult to experimentally quantify. In addition to the TEM investigation of Legros *et al.* [7] and Tang *et al.* [11], a NMR study of deuterium in deformed Pd was performed by Baukraa *et al.* at large ($x \sim 0.6$) deuterium solute concentration [17]. While low activation energy consistent with deuterium DPD was deduced, the authors concluded significant site blocking existed at dislocations, completely inhibiting solute transport. Thus, the diffusivity was not quantified. In fact, no direct measurement of DPD $D(T)$ exists since all published TEM work requires the application of a transport model to determine diffusivity. QENS provides a direct measurement of residence time and jump distance of the diffusing species. The large incoherent neutron scattering cross section of hydrogen allows QENS measurements at the low solute concentrations necessary to separate the migration of trapped solute atoms from regular bulk diffusion.

The time-of-flight neutron backscattering silicon spectrometer (BASIS) at the Spallation Neutron Source at Oak Ridge National Laboratory [18] and the High-Flux Backscattering Spectrometer (HFBS) at the National Institute of Standards and Technology Center for Neutron Research [19] were used to quantify trapped hydrogen kinetics with QENS. The sample material for

the BASIS and HFBS experiments was 0.25-mm-thick 99.98% pure (metals basis) cold-rolled polycrystalline Pd sheet supplied by Alpha Aesar identical to that used previously for vibrational density of state measurements of trapped hydrogen [20–22]. In addition to the deformation by cold rolling, the deformed samples were cycled across the Pd-H miscibility gap (hydride cycling) to introduce additional dislocations using the procedure described in Ref. [23]. The resulting dislocation substructure is characterized by a cellular network (the response to cold working) and a more uniform distribution within the cell interiors (the response from hydride cycling) [23]. Four samples were studied, two deformed samples on BASIS (Def-1 and Def-2), one well-annealed sample on BASIS (Ann-1), and one well-annealed sample on HFBS (Ann-2). The relevant characteristics of these samples are listed in Table I. Additional information regarding QENS instrument characteristics, sample preparation, and QENS measurement procedures can be found in the Supplemental Material [24].

An example of the effect of temperature on the QENS response is shown in Fig. 1 for the Def-1 sample. The measured QENS response is due to hydrogen transport since the self-diffusion of Pd is effectively zero at ambient T [27]. The inset shows the drop in elastic peak intensity as the temperature increases, corresponding to the increase in QENS intensity observed beyond the elastic limit. This increase in QENS intensity is due to thermally activated hydrogen diffusion. The zero-phonon or measured QENS intensity is proportional to the incoherent dynamic structure factor, $S_{inc}(Q,\omega)$, which is related to the double differential incoherent neutron scattering cross section via

$$\frac{d^2\sigma}{d\Omega d\omega} = \frac{\sigma_{inc}}{4\pi}\frac{k}{k_0}S_{inc}(\boldsymbol{Q},\omega), \tag{1}$$

where k_0 and k are the incident and scattered wave vector, respectively, and σ_{inc} is the incoherent neutron scattering cross section. The most general form of $S(\boldsymbol{Q},\omega)$ contains correlations between the same nucleus at different times (incoherent scattering) and correlations between different nuclei at different times (interference effects associated with coherent scattering, both elastic and inelastic). The incoherent dynamic structure factor is given in general form as

$$S_{inc}(\boldsymbol{Q},\omega) = e^{-\hbar\omega/2kT}\left[e^{-2W}\left(A_0(\boldsymbol{Q})\delta(\omega) + \sum_{j=1}^{n}A_j(\boldsymbol{Q})L_j(\boldsymbol{Q},\omega)\right) \otimes R(\boldsymbol{Q},\omega) + B(\boldsymbol{Q},\omega)\right], \tag{2}$$

where $e^{-\hbar\omega/2kT}$ is a detailed balance factor, the product $A_0\delta(\omega)$ is the elastic contribution, the products A_jL_j are the quasielastic contributions, and $B(Q,\omega)$ is the background. A_0 and A_j are referred to as the elastic and quasielastic incoherent structure factors, respectively. The elastic and quasielastic intensity contributions are convoluted with the instrument resolution function $R(Q,\omega)$ and attenuated by the Debye-Waller factor e^{-2W} [28].

We are concerned with diffusive motion of hydrogen solutes in a crystal lattice: incoherent inelastic scattering. The quasielastic contribution to the dynamic structure factor for discrete translational jumps is given by a single Lorentzian function [15],

$$L(\boldsymbol{Q},\omega) = \frac{1}{\pi}\frac{f(\boldsymbol{Q})}{f(\boldsymbol{Q})^2+\omega^2}, \tag{3}$$

where $f(\mathbf{Q})$ is the Lorentzian half-width. The orientation-average width $f(\mathrm{Q})$ for jump distance l on a Bravais lattice is given by [15]

$$\hbar f(Q) = \hbar\omega_L = E_L = \frac{\hbar}{\tau}\left(1-\frac{\sin(Ql)}{Ql}\right), \tag{4}$$

where τ is the residence time associated with the translational diffusive jumps. The diffusion coefficient is given by the Einstein equation for three-dimensional random motion, $D = l^2/(6\tau)$.

The best fits in Fig. 1 represent a convolution of the resolution function with a single Lorentzian, an elastic component, and a background term, as presented in Eq. (2). The instrumental resolution function is sample dependent [18]. Accordingly, the lowest temperature measurement ($T \leq 25$ K, see Table 1) for each sample measured on BASIS was used for $R(Q,\omega)$. The statistical uncertainty of the corresponding HFBS 20-K measurement was too large,

TABLE I. QENS sample characteristics and Arrhenius fit results for $D(T) = D_0\exp(-E_a/\mathrm{k}T)$.

Sample	Mass [g]	C_H[H]/[Pd]	H inventory [mg]	T points [K]	D_0[cm^2/s]	E_a [eV]
Def-1	116	1.13×10^{-3}	1.2	20, 150, 200, 250, 300	$9(3)\times10^{-6}$	0.083 ± 0.005
Def-2	311	0.52×10^{-3}	1.5	15, 220, 260,300, 350	$10(5)\times10^{-6}$	0.042 ± 0.012
Def-1	116	1.13×10^{-3}	1.2	350, 400		
Ann-1	116	2.02×10^{-3}	2.2	25, 200,[a] 280, 350	0.005 ± 0.004	0.23 ± 0.02
Ann-2	59	3.33×10^{-3}	1.8	300,[b] 400[b]		

[a]The 200-K measurement of Ann-1 exhibited no measureable QENS broadening; the dynamics associated with known diffusivity at this temperature in well-annealed Pd are within the instrumental resolution.
[b]HFBS measurement; all other samples measured on BASIS.

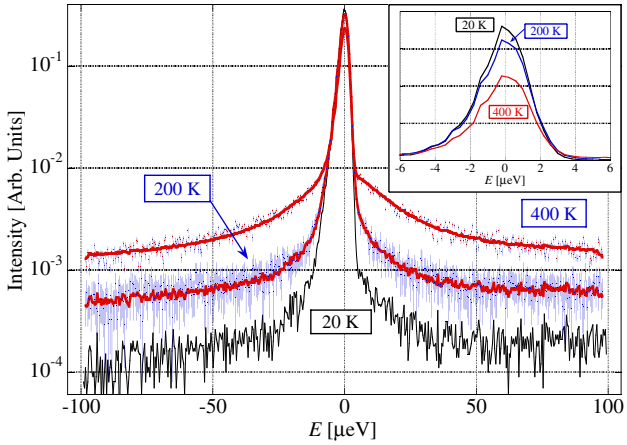

FIG 1 (color online). Fits to intensity versus energy transfer in the QENS region (the $Q = 0.9$ Å^{-1} bin) for Def-1 at 200 and 400 K, as explained in the text. The 20-K measurement quantifies the instrumental resolution, which is sample dependent [18], since all motions are assumed to be frozen. The 200-and 400-K plotting symbols are the $\pm 1\sigma$ error bars associated with each data point. The decrease in elastic intensity is shown in the inset (linear intensity scale) and corresponds to an increase in the QENS response.

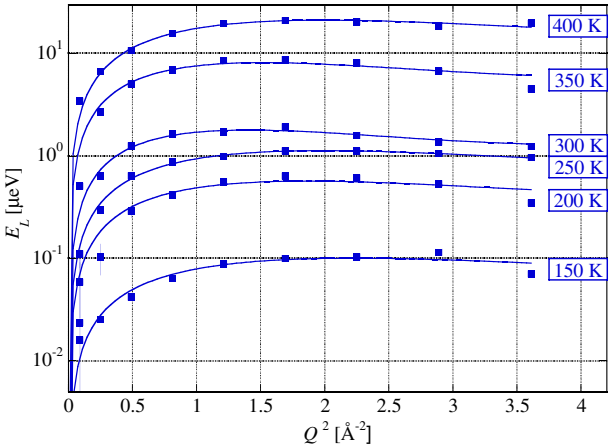

FIG 2 (color online). Fits of the Chudley-Elliot model [Eq. (4)] to the Def-1 sample Lorentzian widths E_L for all temperatures. Widths E_L are shown on a log scale to highlight the significant variation in Lorentzian widths versus T. The experimental uncertainties in all E_L values are approximately 10% fractional error.

and vanadium (a nearly pure incoherent scatterer) was used. Most intensity versus E sets could be fit with a single Lorentzian; however, some low-T sets of Def-1 required two, with a second much broader ($E_L \sim 10^2$ μeV) component with a Q-independent width. The lack of Q dependence and larger width implies a fast localized process not associated with diffusion via translational jumps. Fits of Eq. (4) to the Def-1 sample widths $E_L(Q)$ are shown in Fig. 2. Similar fits to Def-2, Ann-1, and Ann-2 were obtained. The two fitting parameters τ and l yield the diffusivity at each temperature via the Einstein equation. Large variations in the jump distance l were observed across the data sets, with systematically larger l at high T for the deformed samples [28].

An Arrhenius plot can be constructed for each measured sample and fit with $D(T) = D_0\exp(-E_a/kT)$, as shown in Fig. 3. The diffusion constant (D_0) and activation energy (E_a) for the four measurements are listed in Table 1. The diffusivity obtained for well-annealed Pd (a combination of Ann-1, Ann-2, and the high-T Def-1 measurements, as reflected in Table 1) agrees well with the known behavior, $D(T) = 0.0045\exp(-0.248\ \text{eV}/kT)\ \text{cm}^2/\text{s}$ [29]. We note diffusion *constants* are difficult to accurately quantify in an Arrhenius analysis over a limited lower temperature range since small changes in slope (E_a) lead to significant deviations in the intercept (D_0). Extrapolation of the Ann-1/Ann-2 Arrhenius response to higher temperature demonstrates the 350- and 400-K measurements of the Def-1 sample are dominated by bulk hydrogen diffusion, not hydrogen DPD. Hydrogen de-trapping above $T \sim 300$ K leads to bulk diffusion behavior in deformed Pd, consistent with the elasticity model for hydrogen occupation of dislocation traps in Pd [20]. We therefore include the two highest T measurements of Def-1 in the fit of the bulk hydrogen diffusion Arrhenius.

The diffusivities for hydrogen DPD are characterized by significantly lower E_a, consistent with the underlying concept. The diffusion constant for both deformed samples associated with hydrogen DPD is lower by two to three orders of magnitude compared to regular bulk diffusion. It is difficult to reconcile this observation with site blocking on the octahedral interstitial sublattice in *bulk* Pd hydride. Site blocking could influence the diffusivity since trapped hydrogen is in the hydride phase below approximately 250 K in $PdH_{0.001}$ [20–23,30]. The diffusion constant D_0 includes the probability of neighboring site availability, $1 - x$. This probability is effectively one in dilute interstitial solutions and the activation energy is equal to the interstitial migration energy. In ideally-stoichiometric PdH, hydrogen diffusivity would include both vacancy formation and migration energy on the interstitial sublattice (analogous to hydrogen self-diffusion via exchange with random-walking vacancies). However, Pd hydride is non-stoichiometric ($PdH_x x \sim 0.6$–0.7), except at inordinately high chemical potential or fugacity. The diffusivity of hydrogen in $PdH_{0.70}$ has been measured with NMR over 296 K $\leq T \leq$ 413 K, $D(T) = 9.0 \times 10^{-4}\exp(-0.228\ \text{eV}/kT)\ \text{cm}^2/\text{s}$ [31], indicating site blocking does not play a significant role in hydrogen transport in the hydride phase, with equivalent E_a and D_0 reduced by a factor of four compared to the dilute solid-solution diffusivity. Nelin and Skold also conclude hydrogen diffusivity is not significantly different for the dilute and hydride phases [12]. The significantly lower E_a we observe for hydrogen DPD therefore cannot be attributed to regular bulk diffusion in Pd hydride formed at dislocations. The D_0 values we find for hydrogen DPD must be evidence of a modified diffusion pathway through a core/near-core site network in which *blocking* plays a much greater role compared to bulk Pd hydride. *Ab initio* simulations

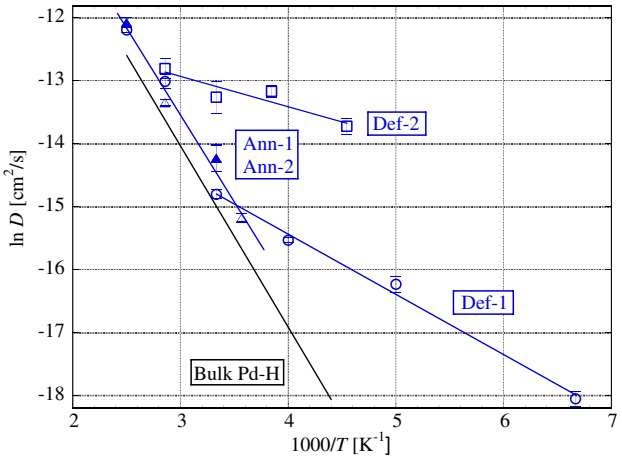

FIG 3 (color online). Arrhenius plot of the hydrogen diffusivities derived from QENS analysis. Blue lines are best fits to the samples analyzed in this work; Def-1 (open circles), Def-2 (open boxes), Ann-1 (open triangles), and Ann-2 (solid triangles). E_a and D_0 values for these fits are listed in Table 1. The thick black line is the expected bulk regular diffusivity of hydrogen in well-annealed Pd from Ref. [29].

presented below provide the physical basis for the DPD pathway and associated blocking.

The $D(T)$ behavior for hydrogen DPD is concentration dependent, with significantly larger diffusivity observed in $PdH_{0.00052}$ compared to $PdH_{0.00113}$. This behavior is due to a $E_a(C_H)$ dependence since the D_0 values for both deformed samples are equal to within experimental uncertainty. A continuum of lattice sites associated with dislocations under tensile strain ε exist, from $\varepsilon \sim 0$ far from dislocations, through $\varepsilon \sim r^{-1}$ at near-core sites (the inverse radial dependence of volumetric strain associated with edge dislocations [32]), to $\varepsilon = 0.05$ at the dislocation core [20,33]. The occupation of these sites by hydrogen is both T and C_H dependent and this occupation dictates the observed E_a for DPD between 150 and 300 K. Hydrogen has lower occupation in the core and near-core sites at lower C_H. We hypothesize this leads to reduced site blocking and a greater sampling of jumps between higher ε sites. The diffusing solutes contributing to the observed QENS response are then characterized by lower E_a since tensile lattice strain reduces the barrier height. This is, in fact, the genesis of the DPD mechanism and the observation of a $E_a(C_H)$ dependence is a demonstration of strain-mediated solute diffusion. Hydrogen de-population of the dislocation trapping sites is exponential with T and this effect influences the diffusion process, leading to the observation of bulk regular diffusion behavior in deformed Pd above 300 K, in agreement with analytical model of Trinkle *et al.* [20].

The preferred hydrogen trapping site is below the edge dislocation partial core in Pd [33]; this site exhibits the largest volumetric strain, but maintains octahedral-like symmetry. Additional *ab initio* calculations have been performed to determine site and diffusion activation barrier energies of hydrogen in the partial dislocation environment of Pd. The computational procedure was the same as that described in Ref. [33]. These energies are shown schematically in Fig. 4. *Ab initio* calculations slightly over estimate the bulk diffusion barrier, $E_a^{\text{bulk}} = 0.27$ eV. The preferred trap sites are part of an octahedral-tetrahedral (O-T) network with trap site energy $E_{\text{trap}} = -0.13$ eV relative to the bulk octahedral interstitial site, $E_{\text{oct}} = 0$. The activation barrier for diffusion along this O-T network is reduced slightly by ΔE so that $E_a^{\text{bulk}} \sim E_a^{\text{trap}}$ and the diffusion along this network does not affect the measured activation energy for diffusion in deformed Pd.

A novel diffusion pathway *inside* the partial core does exist, however. This pathway is comprised of interstitial sites, E_{core} in Fig. 4, that are neither octahedral nor tetrahedral in terms of neighboring Pd atom symmetry. These sites are meta-stable with respect to the O-T network sites by ~30 meV and characterized by a significantly lower activation energy for diffusion, $E_a^{DPD} = 0.11$ eV. This is in good agreement with our Def-1 value. We note E_a^{DPD} is likely a slight over-prediction as well and that small barriers are more susceptible to zero-point motion effects that will lower the effective barrier height. The core DPD sites are directly connected to the trap sites, but *not* to the bulk octahedral sites and this limited interconnectivity allows a hydrogen atom to undergo the following jumps: (a) a jump from a trap site into a core site, (b) jumps within the core associated with DPD, and (c) a jump out of the core back into the trap site, provided the latter is not occupied or blocked. Given the limited number of core and preferred trap sites, we expect a DPD process dependent on both

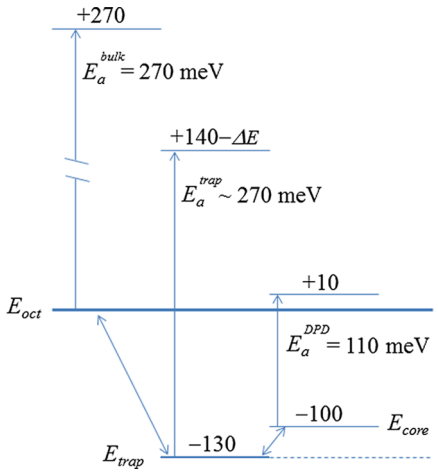

FIG 4 (color online). *Ab initio* results of site and activation energies (in meV) for hydrogen diffusion in the near partial dislocation core environment in Pd, relative to the bulk octahedral interstitial site, $E_{oct} = 0$. ΔE accounts for the slight reduction of the O-T trapping network, as discussed in the text. Vertical arrows indicate diffusion activation energy barriers. The site in the partial core is meta-stable with respect to the preferred trap site that resides just below the partial dislocation [33]. Solute hopping along core sites is associated with DPD, and core sites can only be accessed via the preferred trap sites.

solute concentration and dislocation density. The limited connectivity will influence the DPD process, imparting a restriction on jumps into and out of the core sites. Such jumps represent a small fraction of the total possible jumps involving the preferred trap sites (jumps to more bulklike octahedral sites comprise the majority) and this, we believe, is the origin of the significant reduction in D_0 observed here for DPD. It is not possible to directly investigate the effect of C_H on DPD within the *ab initio* framework to confirm the $E_a(C_H)$ dependence we observed experimentally. We are currently performing kinetic Monte Carlo simulations to investigate C_H dependence on DPD.

Temperature-dependent QENS measurements of trapped hydrogen represent a unique experimental scenario that allows the diffusivity associated dislocation pipe diffusion to be directly quantified. This analysis is not model dependent and relies solely on the assumption of translational diffusion via solute hopping on a Bravais lattice. We confirm the regular bulk diffusivity of hydrogen in well-annealed Pd, thereby eliminating any possible systematic errors associated with the application of QENS. Activation energies associated with hydrogen DPD are significantly lower than the bulk regular diffusion E_a value and are concentration dependent. The hydrogen-DPD diffusion constant is reduced by 2 to 3 orders of magnitude compared to bulk D_0. This is likely due to restrictions of DPD mechanism on the core and preferred trap site hopping network. Hydrogen de-population of trap sites above 300 K leads to bulk regular $D(T)$ behavior in deformed Pd, consistent with an elastic continuum model for hydrogen occupation previously published. *Ab initio* computations confirm the reduced barrier height for DPD observed experimentally and provide a physical basis for the DPD pathway, uncovering an atomistic mechanism involving motion from trap states to "diffusive" core states.

This work was supported by the NSF under Grant No. DMR-1207102, and in part by the NSF through the XSede resources provided by NCSA and TACC. Part of the research presented here was conducted at Spallation Neutron Source, was sponsored by the Scientific User Facilities Division, Office of Basic Energy Sciences, US Department of Energy. This work utilized facilities supported in part by the National Science Foundation under Agreement No. DMR-0944772. Identification of commercial products does not imply endorsement by the National Institute of Standards and Technology nor does it imply that these are the best for the purpose. Finally, we are grateful to Y. Zhang (University of Illinois) for useful discussions regarding QENS analysis.

*bheuser@illinois.edu

[1] D. Turnbull and R. E. Hoffman, Acta Metall. **2**, 419 (1954).
[2] E. W. Hart, Acta Metall. **5**, 597 (1957).
[3] G. R. Love, Acta Metall. **12**, 731 (1964).
[4] T. Volin, K. H. Lie, and R. W. Balluffi, Acta Metall. **19**, 263 (1971).
[5] R. M. Thomson and R. W. Balluffi, J. Appl. Phys. **33**, 803 (1962).
[6] R. W. Balluffi and R. M. Thomson, J. Appl. Phys. **33**, 817 (1962).
[7] R. Kirchheim, Acta Metall. **29**, 835 (1981).
[8] M. Legros, G. Dehm, E. Arzt, and T. J. Balk, Science **319**, 1646 (2008).
[9] Y. Tang and J. A. El-Awady, Phys. Rev. B **86**, 174102 (2012).
[10] Y. Gao, Z. Zhuang, Z. L. Liu, X. C. You, X. C. Zhao, and Z. H. Zhang, Int. J. Plast. **27**, 1055 (2011).
[11] X. Tang, K. P. D. Lagerlof, and A. H. Heuer, J. Am. Ceram. Soc. **86**, 560 (2003).
[12] K. Skold and G. Nelin, J. Phys. Chem. Solids **28**, 2369 (1967); **36**1175 (1975).
[13] J. M. Rowe, J. J. Rush, L. A. de Graaf, and G. A. Ferguson, Phys. Rev. Lett. **29**, 1250 (1972).
[14] M. Bee, *Quasielastic Neutron Scattering: Principles and Applications in Solid State Chemistry, Biology, and Materials Science* (Adam Hilger, Bristol, England, 1988).
[15] C. T. Chudley and R. J. Elliot, Proc. Phys. Soc. **77**, 353 (1961).
[16] K. A. Terrani, E. Mamontov, M. Balooch, and D. R. Olander, J. Nucl. Mater. **401**, 91 (2010).
[17] A. Boukraa, G. A. Styles, and E. F. W. Seymour, J. Phys. Condens. Matter **3**, 2391 (1991).
[18] E. Mamontov and K. W. Herwig, Rev. Sci. Instrum. **82**, 085109 (2011).
[19] A. Meyer, R. M. Dimeo, P. M. Gehring, and D. A. Neumann, Rev. Sci. Instrum. **74**, 2759 (2003).
[20] D. R. Trinkle, H. Ju, B. J. Heuser, and T. J. Udovic, Phys. Rev. B **83**, 174116 (2011).
[21] B. J. Heuser, T. J. Udovic, and H. Ju, Phys. Rev. B **78**, 214101 (2008).
[22] H. Ju, B. J. Heuser, D. L. Abernathy, and T. J. Udovic, Nucl. Instrum. Methods Phys. Res., Sect. A **654**, 522 (2011).
[23] B. J. Heuser and H. Ju, Phys. Rev. B **83**, 094103 (2011).
[24] See Supplemental Material at http://link.aps.org/supplemental/10.1103/PhysRevLett.113.025504 for additional information regarding sample preparation, QENS instrument characteristics, and QENS measurement procedures, which includes Refs. [25] and [26].
[25] F. Fromm and H. Jehn, Bull. Alloy Phase Diagrams **5**, 325 (1984).
[26] G. L. Squires, *Introduction to the Theory of Thermal Neutron Scattering* (Cambridge University Press, Cambridge, England, 1978).
[27] N. L. Peterson, Phys. Rev. **136**, A568 (1964).
[28] See Supplemental Material at http://link.aps.org/supplemental/10.1103/PhysRevLett.113.025504 for the development and application of the Debye-Waller factor to determine mean-square displacements related to the QENS response and for a discussion of the systematically larger jump distances.
[29] H. K. Birnbaum and C. A. Wert, Ber. Bunsen-Ges. Phys. Chem. **76**, 806 (1972).
[30] B. J. Heuser, D. R. Trinkle, T.-N. Yang, and L. L. He, J. Alloys Compd. **577**, 189 (2013).
[31] E. F. W. Seymour, R. M. Cotts, and W. D. Williams, Phys. Rev. Lett. **35**, 165 (1975).
[32] J. P. Hirth and J. Lothe, *Theory of Dislocations* (Wiley, New York, 1982), 2nd ed.
[33] H. M. Lawler and D. R. Trinkle, Phys. Rev. B **82**, 172101, (2010).